

This document is the Accepted Manuscript version of a Published Work that appeared in final form in Nano Letters, copyright © American Chemical Society after peer review and technical editing by the publisher. To access the final edited and published work see <http://pubs.acs.org/articlesonrequest/AOR-Jz3vxXZev3e6IJfEvSn8>.

---

## DOPING MOLECULAR WIRES

**Georg Heimel,<sup>1,2\*</sup> Egbert Zojer,<sup>3</sup> Lorenz Romaner,<sup>4</sup> Jean-Luc Brédas,<sup>5</sup>  
and Francesco Stellacci<sup>2</sup>**

<sup>1</sup> *Institut für Physik, Humboldt-Universität zu Berlin, Newtonstr. 15,  
D-12489 Berlin, Germany;*

<sup>2</sup> *Department of Materials Science and Engineering, Massachusetts Institute of  
Technology, 77 Massachusetts Ave., Cambridge, Massachusetts 02139;*

<sup>3</sup> *Institute of Solid State Physics, Graz University of Technology, Petersgasse 16,  
A-8010 Graz, Austria;*

<sup>4</sup> *Chair of Atomistic Modeling and Design of Materials, University of Leoben,  
Franz-Josef-Strasse 18, A-8700 Leoben, Austria;*

<sup>5</sup> *School of Chemistry and Biochemistry and Center for Organic Photonics and  
Electronics, Georgia Institute of Technology, 901 Atlantic Dr. NW,  
Atlanta, Georgia 30332-0400.*

---

\* To whom correspondence should be addressed: [georg.heimel@physik.hu-berlin.de](mailto:georg.heimel@physik.hu-berlin.de)

## ABSTRACT

The concept of doping inorganic semiconductors enabled their successful application in electronic devices. Furthermore, the discovery of metal-like conduction in doped polymers started the entire field of organic electronics. In the present theoretical study, we extend the concept of doping to monomolecular wires suspended between two metal electrodes. Upon doping, the conductivity of representative model systems is found to increase by two orders of magnitude. More importantly, by providing a thorough understanding of the underlying mechanisms, our results pave the way for the development of novel molecular components envisioned as functional units in nanoscale devices.

The technological relevance and the functionality of semiconducting materials originates in the fact that their conductivity and the band alignment at interfaces with other materials can be controlled through doping. This has ultimately led to the multitude of (opto)electronic devices that impact almost every aspect of modern life. Likewise, the entire field of organic electronics originates in the discovery of metal-like conduction in poly(acetylene) doped with iodine<sup>1, 2</sup> and doping organic semiconductors has been found to enhance the performance of plastic electronic devices.<sup>3, 4</sup> Here, we consider the ultimate miniaturization of such devices and theoretically investigate the doping of molecular wires in single-molecule junctions, where an organic molecule is suspended between two metal electrodes.<sup>5-10</sup> For representative model systems, we find that, upon doping, the molecular conductivity is enhanced by more than two orders of magnitude in the technologically relevant low-bias region. Going significantly beyond previous work,<sup>11, 12</sup> we elucidate the microscopic origin of this dramatic effect and present an intuitive picture which rationalizes our observations in terms of *Fermi-level pinning*.<sup>13-15</sup> The mechanism underlying the doping-induced changes in conductivity is, thus, found to differ markedly from those in both inorganic and organic bulk semiconductors, as it hinges entirely on the re-alignment of the frontier molecular orbitals (MOs) relative to the Fermi level ( $E_F$ ) of metal contacts. Our results permit shedding new light on recent theoretical<sup>11, 12, 16-23</sup> and experimental work.<sup>8-10, 16, 17, 24</sup> Most importantly, however, the provided insights into the working principles of doping pave the way for the rational

design of novel functional components for sensing and switching on the single-molecule scale as well as for the development of highly responsive surfaces and interfaces.

As an instructive example for an entire class of materials, we focus on a molecular wire consisting of a prototypical  $\pi$ -conjugated molecule which, for the purposes of this study, can also be viewed as a small piece of graphene or simply as an intrinsic (*i.e.*, undoped) semiconductor: a dithiol derivative of pyrene where the thiol groups are separated from the  $\pi$ -conjugated core by a methylene (*i.e.*, -CH<sub>2</sub>-) spacer (Fig. 1a). A molecular junction<sup>5-10</sup> is built by contacting this molecule on both sides (*via* replacement of the S-H bonds with S-Au bonds) by a semi-infinite gold electrode (Fig. 1b-c). The electronic structure of the entire system was calculated at the density-functional theory level and the zero-bias transmission of the junction was obtained through the Landauer-Büttiker formalism,<sup>25, 26</sup> *i.e.*, no explicit voltage drop across the junction was considered. As the system is symmetric (Fig. 1), the current through the molecular wire at a given bias voltage,  $V$ , is then given by the integral over the transmission between the symmetric limits of  $E_F \pm e \times V/2$  (with  $e$  denoting the elementary charge), taking into account an electronic temperature of 300 K (see Supporting Information for further details on the system setup and the computational methodology).

To investigate the effect of doping, we first follow the original strategies in the field of conducting polymers. There,  $n$ -type doping has been achieved by exposing the organic semiconductor to alkali metals<sup>2, 12</sup> and  $p$ -type doping through treatment with halogens.<sup>1, 11</sup> Through a redox reaction, the molecules are rendered radical-anions in the

former and radical-cations in the latter case. At high doping levels (on the order of %) the generated charge carriers lead to an increase of the bulk electrical conductivity by several orders of magnitude.<sup>1, 2, 27</sup> Here, we chose a single Na or Cl atom, placed above the central C-C bond of the model molecule (Fig. 1b); the optimized vertical distances to the molecular plane are  $d_{Na} = 2.49 \text{ \AA}$  and  $d_{Cl} = 2.95 \text{ \AA}$ . As expected,<sup>27, 28</sup> we observe pronounced charge transfer between dopant and molecule in both cases (a Mulliken analysis yields  $+0.32 e$  on the  $\text{Na}^+$  and  $-0.32 e$  on the  $\text{Cl}^-$  counter-ion, where  $e$  denotes the elementary charge). In Fig. 2a, the simulated current-voltage characteristic,  $I(V)$ , of the junction is shown for both the undoped and the redox-doped molecule. Most strikingly, the shape of the  $I(V)$  characteristic (below  $\pm 1.2 \text{ V}$ ) qualitatively changes from concave to convex upon doping, the current is seen to increase by up to two orders of magnitude in this low-voltage window, and the transport gap vanishes. However, as discussed in, *e.g.*, Ref. 24, doping molecular wires with only Coulomb-bound counter-ions may not constitute the most practical approach since diffusion of these ions and their drift due to the high electric fields in nanometer-sized junctions can lead to fluctuations in the local geometry and, as a result, to instabilities of the molecular  $I(V)$  characteristics.

In contrast to “external” redox doping, we thus considered next the possibility of “internal” doping: In conventional silicon technology, doping is realized by substituting group-IV silicon atoms in the crystal lattice with group-V elements (*e.g.*, P) for  $n$ -type and group-III elements (*e.g.*, B) for  $p$ -type doping. At finite temperature, group-V atoms can donate an electron into the conduction band of the semiconductor while group-III

atoms can inject a hole into the valence band; through this mechanism, the concentration of free charge carriers is increased and, consequently, the electrical conductivity of the material rises dramatically. Similarly to this scenario and in a way reminiscent also of the doping of carbon nanotubes,<sup>29-31</sup> we replace one of the two (symmetry-equivalent) central C-atoms (4 valence electrons) in our model molecule with nitrogen or boron (Fig. 1c).<sup>32</sup> Nitrogen, having 5 valence electrons, adds an extra electron (*n*-doping) into the lowest unoccupied molecular orbital (LUMO) of the molecule in the junction, *i.e.*, the “conduction band” of the single-molecule semiconductor. Boron, with 3 valence electrons, adds an additional hole (*p*-doping) into the “valence band” of the molecular wire, *i.e.*, its highest occupied molecular orbital (HOMO). Since, in contrast to doping with Cl<sup>-</sup> or Na<sup>+</sup>, the molecule remains electrically neutral, no counter-ions are required to stabilize the unpaired electron. Interestingly, the increase in current through the N- and B-doped molecular wires at low bias (below  $\pm 1.2$  V) is calculated to be even more pronounced (Fig. 2b) than in the case of redox doping (Fig. 2a). Again, the shape of the  $I(V)$  characteristic qualitatively changes from concave to convex and the transport gap vanishes.

To rationalize this dramatic increase in conductivity, it is helpful to first analyze the electronic structure of the undoped molecule in the junction. The density of states *projected* onto the molecular region (PDOS) is shown in the left panel of Fig. 3a for that case. A peak is observed at  $\approx 0.6$  eV below and  $\approx 1.8$  eV above  $E_F$ . The right panel of Fig. 3a shows the 3D representations of the *local* density of states (LDOS), *i.e.*, the

number of states per volume element and energy interval, integrated over a  $\pm 30$  meV energy window around these peaks. The densities are fully delocalized across the junction and, in the region of the molecule, they can be identified as originating from its HOMO and LUMO, respectively. In contrast, around  $E_F$ , significant density is found only within the metal and none is seen on the molecular core. As expected, the calculated transmission  $T(E)$ , *i.e.*, the “transparency” of the junction for an incident ballistic electron with energy  $E$ , exhibits a sharp peak (Fig. 3b) at the HOMO energy ( $\approx -0.6$  eV) as the electronic states at that energy fully bridge the gap between the electrodes (Fig. 3a). The resulting  $I(V)$  characteristics of the undoped molecule and, in particular, its transport gap (Fig. 2) can now be understood: The current stays low until the HOMO enters the bias window (around  $\pm 1.2$  V in the symmetric junction assumed here) and then rises sharply as a continuous transport channel becomes available (Fig. 3). Qualitatively, the situation described above is encountered in most molecular junctions:<sup>5-10</sup>  $E_F$  lies within the energy gap of a closed-shell molecular wire, its doubly occupied HOMO lies well below  $E_F$ , and the empty LUMO lies above; one observes very low current at low bias and a non-linear increase of the current at higher voltage as transmission channels successively become available.

Importantly, the energy of the ionization and affinity levels of the free molecule *prior* to contact with the metal are largely inconsequential for the level alignment *after* contact. Bond formation between metal and molecule gives rise to interfacial potential steps that shift the frontier MOs in energy.<sup>33-36</sup> Their final alignment relative to the Fermi

level depends on the chemical “anchoring” group<sup>35, 37-41</sup> and on atomistic details of the docking geometry<sup>38, 42-44</sup> as long as  $E_F$  remains well within the molecular gap. Should, however,  $E_F$  approach one of the frontier MOs, then the mechanism sketched in Fig. 4a starts dominating the interface energetics: Starting with, *e.g.*, the Fermi level close to the fully occupied HOMO would lead to occupied states on the molecule above  $E_F$  (left panel). As the electron chemical potential equilibrates, charge flows from molecule to metal (center panel). Even small amounts of charge transfer between the metal and the delocalized HOMO (extending to far above the metal surface) result in appreciable dipole moments. These give rise to interfacial potential steps,<sup>33-36</sup> which push the now somewhat emptied HOMO down below  $E_F$  (right panel). The Fermi level is *pinned*<sup>13-15</sup> to the HOMO *onset*. In other words, the delocalized frontier MOs of linear closed-shell molecular wires “standing” on an electrode surface cannot easily be moved into resonance with  $E_F$ .<sup>23, 39-50</sup>

The scenario changes drastically upon doping. As, in principle, internally doped systems can be expected to be of higher practical relevance (*vide supra*), we focus in the following on the nitrogen- and boron-doped molecular wires. However, the rationale below equally applies to the Cl<sup>-</sup> and Na<sup>+</sup>-doped cases (see Supporting Information). In the calculated PDOS of the N- and B-doped molecules (Fig. 5), a peak is now found virtually in resonance with  $E_F$  in both instances (46 meV above and 22 meV below  $E_F$ , respectively). Visualization of the LDOS around  $E_F$  (Fig. 5) reveals that, in contrast to the undoped molecule (Fig. 3a), a continuous transport channel is available at that energy;

the electronic states in the gold leads around the Fermi level now extend across the entire junction, *i.e.*, their metallic character “spills over” onto the doped molecule. The presence of fully delocalized states around  $E_F$  manifest itself in a pronounced transmission peak close to that energy and  $T(E_F)$  is more than two orders of magnitude higher for the N- and B-doped molecules than for the undoped closed-shell system (Fig. 3b). The availability of such transport channels already at vanishing bias causes the steep initial increase in  $I(V)$  and the disappearance of the transport gap observed in Fig. 2b. As soon as the entire transmission feature lies within the bias window (at *ca.*  $\pm 0.3$  V), the current through the junction is a factor of 200 higher than in the case of the undoped molecule (Fig. 2b) in the same low-voltage regime.<sup>51</sup>

Interestingly, the PDOS peak at  $E_F$  in the N-doped case (Fig. 5) is related to the LUMO of the undoped molecule (Fig. 3a) and the peak at  $-2.2$  eV clearly corresponds to its HOMO. In essence, the frontier MOs the N-doped system are shifted down in energy (by  $\approx 1.7$  eV) whereas the levels of the B-doped molecule are lifted up (by  $\approx 0.5$  eV) with respect to the undoped situation.<sup>52</sup> Importantly, these shifts *cannot* arise from doping-induced changes in the HOMO- or LUMO-energies of the free molecule,<sup>34-36</sup> as these are calculated to be less than  $\pm 0.08$  eV. A fundamentally different mechanism is at work here: In contrast to the undoped species, the doped molecules are radicals, *i.e.*, they contain an odd number of electrons (open-shell systems) and their highest MO is only singly occupied (SOMO). In the case of  $\text{Cl}^-$  and  $\text{Na}^+$ -doping, the entire counter-ion/molecule charge-transfer complex should be seen as one radical species; the only

partially charged (*vide supra*) molecular wire by itself cannot, strictly speaking, be regarded as radical-ion. The internally doped systems are *neutral radicals*. In contrast to the closed-shell situation discussed above, occupied states on the molecule are now only encountered above the Fermi level if the SOMO *peak* were slightly above  $E_F$  (Fig. 4b, left panel). Then, charge flows from radical to metal (Fig. 4b, center panel). Owing to the high molecular density of states at energies around the SOMO and due to its extension to far above the metal surface, already vanishing amounts of charge transfer can give rise to sizeable interface dipoles. The resulting potential steps push the SOMO back down in energy to reach the equilibrium situation where  $E_F$  lies right *at* the SOMO peak (Fig. 4b, right panel). In other words, the delocalized SOMO of linearly extended radicals “standing” on a metal electrode is efficiently *pinned*<sup>13-15</sup> at  $E_F$  due to its single occupation (see Supporting Information for a discussion of spin polarization).<sup>23, 39-50</sup> Ideally, this should be the case regardless of docking chemistry or atomistic details of the metal/molecule contact geometry.

In the following, we discuss recent observations in view of the doping mechanism outlined above. For cobaltacene-based molecular wires, Liu *et al.* have reported pronounced transmission peaks around  $E_F$ .<sup>20-23</sup> In contrast, for ferrocene compounds,  $E_F$  was found to lie well within the molecular gap.<sup>20, 22</sup> While these findings have been rationalized on the basis of the respective MO energies,<sup>21, 22</sup> our results point towards a different origin of the observed energy-level alignment: Cobaltocene is a neutral radical with Co contributing the unpaired electron; in such a situation, the SOMO

is pinned at  $E_F$  (Fig. 4b). Ferrocene, on the other hand, is *a priori* a closed-shell system and, therefore,  $E_F$  must be expected to lie within the molecular gap (Fig. 4a).<sup>17, 53</sup> Remarkably, the data on cobaltocene presented in Ref. 23 indicate that the energetic position of the SOMO (pinned at  $E_F$ ) is indeed insensitive to atomistic details in the contact geometry at the metal/molecule interface, which is generally not the case for the alignment of  $E_F$  with the frontier MOs of closed-shell molecular wires.<sup>38, 42-44</sup> This further supports the notion that pinning is indeed the dominant driving force for the interfacial energy-level alignment in these systems (*vide supra*).

Another potentially affected area are single-molecule transport measurements under electrochemical potential control.<sup>8-10, 16, 24</sup> There, changes in the molecular conductivity with applied overpotential are usually explained in terms of a continuous tuning of the energy offset between the Fermi level of the metallic contacts and the frontier MOs of the molecular wire. Although the experimentally encountered situation is certainly more complex than the scenario of redox-doping discussed above (Figs. 1b and 2a), our findings suggest an alternative interpretation: Varying the potential of the contacts changes the concentration of ions present in the molecular junction. It has been shown previously<sup>18, 19, 54</sup> that co-adsorption of ions on the electrodes can impact the interfacial energy-level alignment and, moreover, ions in the junction are likely to oxidize/reduce the molecular wire. Notably, our results (Figs. 1b and 2a) indicate that this causes a re-alignment of its frontier MOs with the Fermi level of the contacts and can, thus, give rise to sizeable variations<sup>8-10, 16</sup> (or fluctuations<sup>24</sup>) of the current through the

junction. (see Supporting Information for an extended discussion including the effects of multiple doping).

To summarize, as opposed to conventional organic and inorganic semiconductors, it is not the increase in free charge carriers but the pinning of partially filled orbitals to the electrode Fermi level that gives rise to the doping-induced conductivity increase in molecular wires. Thus, *neutral* radicals in particular, can be regarded as the single-molecule analog to degenerately doped semiconductors (*i.e.*,  $E_F$  within the conduction or valence band) or metals (*i.e.*, high DOS around the Fermi level and Ohmic contact). In addition to more apparent guidelines for the design of desirable neutral radicals (*e.g.*, structural rigidity and the presence of chemical anchoring groups<sup>5-7</sup>), we emphasize that their SOMO must be delocalized over the entire molecular backbone to provide a continuous transport channel between the electrodes. Note that the neutral radicals discussed here were chosen to most clearly convey the mechanism of doping and its underlying principles; removing, *e.g.*, the methylene linkers between the pyrene core and the thiol groups leads to the charge rearrangements occurring upon metal/molecule bonding to compete with the pinning mechanism discussed above (*cf.* Ref. 23). More rewarding synthetic targets could be based, *e.g.*, on the structures recently proposed by Crivillers *et al.*<sup>55</sup> or on organo-metallic transition-metal complexes with  $\pi$ -conjugated ligands (which are of interest also for molecular spintronics).<sup>17, 20-23, 56</sup>

Such molecules can serve as low-resistance interconnects in nano-scale electronics and other applications, *e.g.*, in “metallic paints” on the basis of metal

nanoparticles solubilized with a ligand shell of this type. While the process of doping expounded here might bear relevance for the development of graphene-based electronics (in terms of, *e.g.*, atomic-scale *p-n* junctions), the major potential for neutral radicals lies in sensing and switching at the single-molecule level: Manipulating the (de)localization of the SOMO via interaction with electric fields or relevant analytes as well as oxidizing/reducing or (de)protonating the neutral radical species can be expected not only to switch the low-bias molecular conductivity over many orders of magnitude, but also to significantly impact the (opto)electronic surface properties of a supporting substrate. Finally, self-assembled monolayers of highly conducting molecular wires can facilitate electrically contacting living cells, which is challenging with untreated metals or semiconductors due to their bio-incompatibility.

## **ACKNOWLEDGEMENTS**

GH acknowledges financial support through the INSANE project (Marie-Curie OIF contract no. 021511). The work at Georgia Tech has been supported by the National Science Foundation, primarily under the MRSEC Program (Award Number DMR-0212302) as well as under the CRIF Program (Award Number CHE-0443564). The authors thank S. Duhm and I. Salzmann for stimulating discussion.

**Supporting Information Available:** System setup and Methodology, data and discussion for Na<sup>+</sup>- and Cl<sup>-</sup>-doped molecular wires, data and discussion of multiple

doping, and spin-polarized calculations. This material is available free of charge via the Internet at <http://pubs.acs.org>.

## REFERENCES

- (1) Shirakawa, H.; Louis, E. J.; MacDiarmid, A. G.; Chiang, C. K.; Heeger, A. J. *J. Chem. Soc., Chem. Commun.* **1977**, 578-580.
- (2) Chiang, C. K.; Druy, M. A.; Gau, S. C.; Heeger, A. J.; Louis, E. J.; MacDiarmid, A. G.; Park, Y. W.; Shirakawa, H. *J. Am. Chem. Soc.* **1978**, *100*, 1013-1015.
- (3) Blochwitz, J.; Pfeiffer, M.; Fritz, T.; Leo, K. *Appl. Phys. Lett.* **1998**, *73*, 729-731.
- (4) Kido, J.; Matsumoto, T. *Appl. Phys. Lett.* **1998**, *73*, 2866-2868.
- (5) Reed, M. A.; Zhou, C.; Muller, C. J.; Burgin, T. P.; Tour, J. M. *Science* **1997**, *278*, 252-254.
- (6) Cui, X. D.; Primak, A.; Zarate, X.; Tomfohr, J.; Sankey, O. F.; Moore, A. L.; Moore, T. A.; Gust, D.; Harris, G.; Lindsay, S. M. *Science* **2001**, *294*, 571-574.
- (7) Xu, B.; Tao, N. J. *Science* **2003**, *301*, 1221-1223.
- (8) Zhang, J.; Chi, Q.; Kuznetsov, A. M.; Hansen, A. G.; Wackerbarth, H.; Christensen, H. E. M.; Andersen, J. E. T.; Ulstrup, J. *J. Phys. Chem. B* **2002**, *106*, 1131-1152.
- (9) Tao, N. J. *Nat. Nanotech.* **2006**, *1*, 173-181.
- (10) Chen, F.; Hihath, J.; Huang, Z. F.; Li, X. L.; Tao, N. J. *Annu. Rev. Phys. Chem.* **2007**, *58*, 535-564.
- (11) Tagami, K.; Tsukada, M.; Wada, Y.; Iwasaki, T.; Nishide, H. *J. Chem. Phys.* **2003**, *119*, 7491-7497.

- (12) Belosludov, R. V.; Farajian, A. A.; Baba, H.; Mizuseki, H.; Kawazoe, Y. *Jpn. J. Appl. Phys* **2005**, *44*, 2823-2825.
- (13) Bardeen, J. *Phys. Rev.* **1947**, *71*, 717-727.
- (14) Tersoff, J. *Phys. Rev. Lett.* **1984**, *52*, 465-468.
- (15) Vásquez, H.; Flores, F.; Oszwaldowski, R.; Ortega, J.; Pérez, R.; Kahn, A. *Appl. Surf. Sci.* **2004**, *234*, 107-112.
- (16) Pobelov, I. V.; Li, Z.; Wandlowski, T. *J. Am. Chem. Soc.* **2008**, *130*, 16045-16054.
- (17) Getty, S. A.; Engtrakul, C.; Wang, L.; Liu, R.; Ke, S. H.; Baranger, H. U.; Yang, W.; Fuhrer, M. S.; Sita, L. R. *Phys. Rev. B* **2005**, *71*, 241401.
- (18) Geng, W. T.; Kondo, H.; Nara, J.; Ohno, T. *Phys. Rev. B* **2005**, *72*, 125421.
- (19) Lang, N. D.; Avouris, P. *Nano Lett.* **2002**, *2*, 1047-1050.
- (20) Liu, R.; Ke, S. H.; Baranger, H. U.; Yang, W. T. *J. Am. Chem. Soc.* **2006**, *128*, 6274-6275.
- (21) Liu, R.; Ke, S. H.; Yang, W. T.; Baranger, H. U. *J. Chem. Phys.* **2006**, *124*, 024718.
- (22) Liu, R.; Ke, S.-H.; Baranger, H. U.; Yang, W. *Nano Lett.* **2005**, *5*, 1959-1962.
- (23) Liu, R.; Ke, S.-H.; Yang, W.; Baranger, H. U. *J. Chem. Phys.* **2007**, *127*, 141104.
- (24) He, H. X.; Li, X. L.; Tao, N. J.; Nagahara, L. A.; Amlani, I.; Tsui, R. *Phys. Rev. B* **2003**, *68*, 045302.
- (25) Landauer, R. *IBM J. Res. Dev.* **1957**, *1*, 223-231.

- (26) Büttiker, M.; Imry, Y.; Landauer, R.; Pinhas, S. *Phys. Rev. B* **1985**, *31*, 6207-6215.
- (27) Brédas, J. L.; Thémans, B.; Fripiat, J. G.; André, J. M.; Chance, R. R. *Phys. Rev. B* **1984**, *29*, 6761-6773.
- (28) Irle, S.; Lischka, H.; Eichkorn, K.; Ahlrichs, R. *Chem. Phys. Lett.* **1996**, *257*, 592-600.
- (29) Stephan, O.; Ajayan, P. M.; Colliex, C.; Redlich, P.; Lambert, J. M.; Bernier, P.; Lefin, P. *Science* **1994**, *266*, 1683-1685.
- (30) Burch, H. J.; Davies, J. A.; Brown, E.; Hao, L.; Contera, S. A.; Grobert, N.; Ryan, J. F. *Appl. Phys. Lett.* **2006**, *89*, 143110.
- (31) Hsu, W. K.; Firth, S.; Redlich, P.; Terrones, M.; Terrones, H.; Zhu, Y. Q.; Grobert, N.; Schilder, A.; Clark, R. J. H.; Kroto, H. W.; Walton, D. R. M. *J. Mater. Chem.* **2000**, *10*, 1425-1429.
- (32) Tagami, K.; Wang, L.; Tsukuda, M. *Nano Lett.* **2004**, *4*, 209-212.
- (33) Heimel, G.; Romaner, L.; Bredas, J. L.; Zojer, E. *Surf. Sci.* **2006**, *600*, 4548-4562.
- (34) Heimel, G.; Romaner, L.; Bredas, J. L.; Zojer, E. *Phys. Rev. Lett.* **2006**, *96*, 196806.
- (35) Heimel, G.; Romaner, L.; Zojer, E.; Bredas, J. L. *Nano Lett.* **2007**, *7*, 932-940.
- (36) Heimel, G.; Romaner, L.; Zojer, E.; Brédas, J. L. *Acc. Chem. Res.* **2008**, *41*, 721-729.

- (37) Zangmeister, C. D.; Robey, S. W.; van Zee, R. D.; Kushmerick, J. G.; Naciri, J.; Yao, Y.; Tour, J. M.; Varughese, B.; Xu, B.; Reutt-Robey, J. E. *J. Phys. Chem. B* **2006**, *110*, 17138-17144.
- (38) Ke, S. H.; Baranger, H. U.; Yang, W. T. *J. Am. Chem. Soc.* **2004**, *126*, 15897-15904.
- (39) Seminario, J. M.; De la Cruz, C. E.; Derosa, P. A. *J. Am. Chem. Soc.* **2001**, *123*, 5616-5617.
- (40) Xue, Y. Q.; Ratner, M. A. *Phys. Rev. B* **2004**, *69*, 085403.
- (41) Lang, N. D.; Avouris, P. *Phys. Rev. B* **2001**, *64*, 125323.
- (42) Ke, S. H.; Baranger, H. U.; Yang, W. T. *J. Chem. Phys.* **2005**, *122*, 074704.
- (43) Ke, S. H.; Baranger, H. U.; Yang, W. T. *J. Chem. Phys.* **2005**, *123*, 114701.
- (44) Xue, Y. Q.; Ratner, M. A. *Phys. Rev. B* **2003**, *68*, 115407.
- (45) Romaner, L.; Heimel, G.; Gruber, M.; Bredas, J. L.; Zojer, E. *Small* **2006**, *2*, 1468-1475.
- (46) As the magnitude of the charge-transfer induced interfacial potential steps is proportional to the distance over which charge is transferred and inversely proportional to the lateral area (*i.e.*, the “footprint” of the molecule) exceptions are found for (a) very short molecular wires<sup>23, 39-45</sup> and (b) for laterally extended molecules lying flat on a metal surface.<sup>47-50</sup> Substantial electron back-transfer between metal and chemical anchoring groups on the molecule is often observed in these cases, which further allows shifting the frontier MOs into/through  $E_F$  with only minor charging of the molecule.<sup>45, 50</sup>

- (47) Hauschild, A.; Karki, K.; Cowie, B. C. C.; Rohlfing, M.; Tautz, F. S.; Sokolowski, M. *Phys. Rev. Lett.* **2005**, *95*, 209602.
- (48) Glowatzki, H.; Broker, B.; Blum, R. P.; Hofmann, O. T.; Vollmer, A.; Rieger, R.; Müllen, K.; Zojer, E.; Rabe, J. P.; Koch, N. *Nano Lett.* **2008**, *8*, 3825-3829.
- (49) Hofmann, O. T.; Rangger, G. M.; Zojer, E. *J. Phys. Chem. C* **2008**, *112*, 20357-20365.
- (50) Romaner, L.; Heimel, G.; Bredas, J. L.; Gerlach, A.; Schreiber, F.; Johnson, R. L.; Zegenhagen, J.; Duhm, S.; Koch, N.; Zojer, E. *Phys. Rev. Lett.* **2007**, *99*, 256801.
- (51) That the current through the neutral radicals reaches twice the value for the intrinsic molecule above the threshold voltage in the latter ( $V > 1.2$  V), can be attributed to the fact that in both N- and B-doped species, a second transport channel becomes available immediately after the SOMO itself (double peaks in Fig. 3b and Fig. 5 around  $E_F$ ).
- (52) The molecular gap is slightly reduced (from  $\approx 2.4$  eV to  $\approx 2.2$  eV which we attribute to stabilization of the partially occupied LUMO (N-doping) and to destabilization of the partially occupied HOMO (B-doping).
- (53) In Ref. 17, the ferrocene moiety is linked to the electrodes via extended  $\pi$ -conjugated segments. Each of the two organic ligands (linker unit with corresponding cyclopentadienyl ring) is a neutral radical by itself. As their mutual coupling through the central iron atom is reduced in this scenario, they separately align their SOMO to the Fermi level of the respective electrode. Consequently, a

conductance peak is found around  $E_F$  also for a formally closed-shell molecular wire.

- (54) Yang, Z.; Lang, N. D.; Di Ventra, M. *Appl. Phys. Lett.* **2003**, *82*, 1938-1940.
- (55) Crivillers, N.; Mas-Torrent, M.; Vidal-Gancedo, J.; Veciana, J.; Rovira, C. *J. Am. Chem. Soc.* **2008**, *130*, 5499-5506.
- (56) Yu, L. H.; Keane, Z. K.; Ciszek, J. W.; Cheng, L.; Tour, J. M.; Baruah, T.; Pederson, M. R.; Natelson, D. *Phys. Rev. Lett.* **2005**, *95*, 256803.

## FIGURE CAPTIONS

**Figure 1.** (a) Chemical structure of the investigated molecule, (b) geometry of the undoped and Cl<sup>-</sup> as well as Na<sup>+</sup>-doped species in the molecular junction, and (c) geometry of the N- and B-doped molecule in the junction.

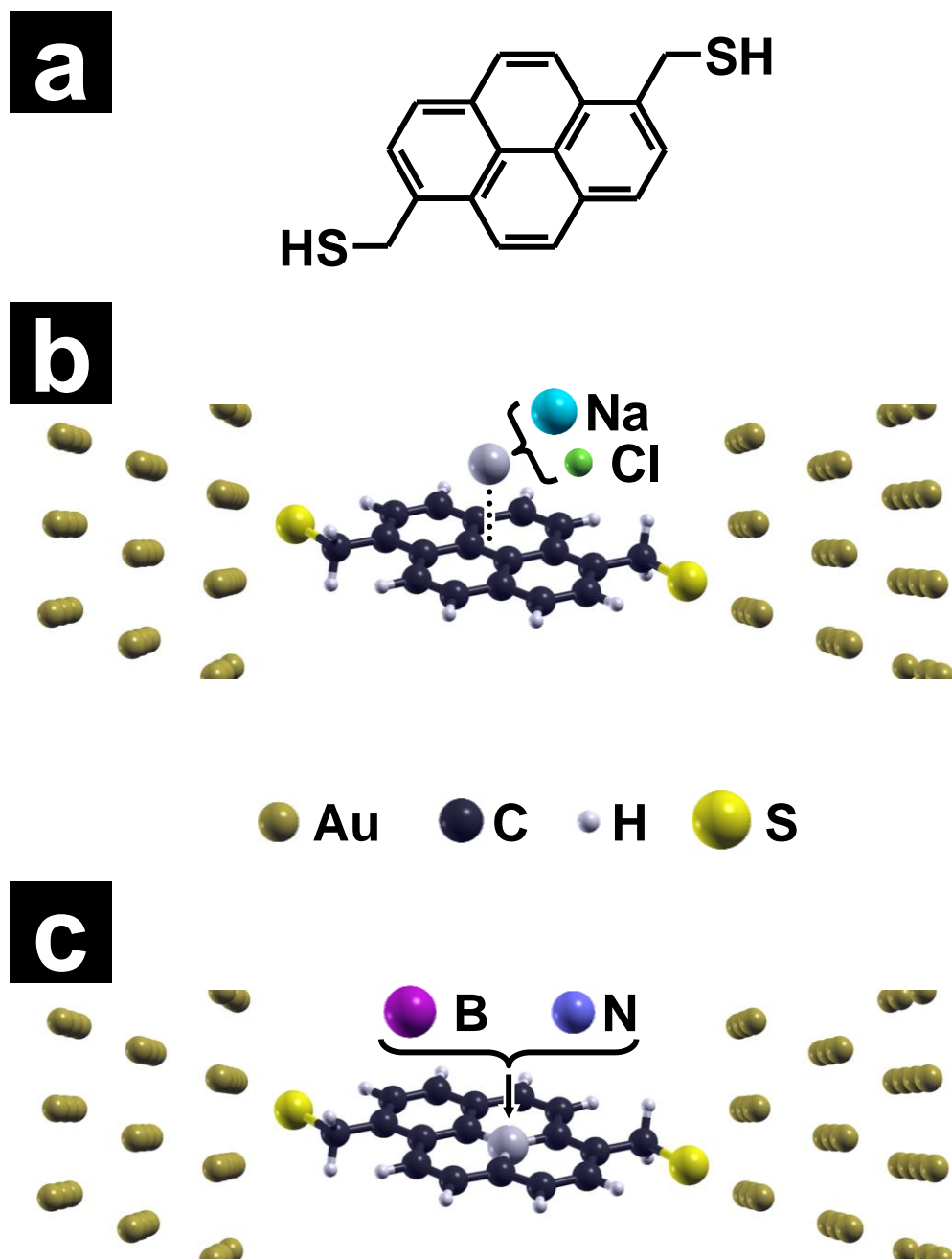
**Figure 2.** (a) Calculated current-voltage characteristics,  $I(V)$ , of the undoped, Cl<sup>-</sup>, and Na<sup>+</sup>-doped molecule and (b) calculated  $I(V)$  characteristics of the undoped, N-, and B-doped molecule.

**Figure 3.** (a) Calculated density of states (in arbitrary units) projected onto the molecular region (PDOS) of the junction containing the undoped molecule (left panel); the origin of the energy scale is the common Fermi level ( $E_F$ ) of the system. The right panels show the local density of states integrated over a  $\pm 30$  meV energy window around the peak indicated HOMO in the left panel (bottom, red), around  $E_F$  (center, orange), and the LUMO peak (top, blue). (b) Calculated transmission function,  $T(E)$ , for the undoped (grey) as well as the N-doped (blue) and B-doped (violet) molecules; the vertical line indicates the position of  $E_F$ .

**Figure 4.** Schematic of the mechanism of energy-level alignment at the metal/molecule interface for (a) closed-shell molecular wires and (b) monoradicals. (a) From left to right: (i) When the highest occupied orbital (HOMO) of the molecular wire approaches the Fermi level ( $E_F$ ) of the electrode, occupied states are found on the molecule above  $E_F$ . (ii) Charge flows from the molecule into the metal to establish a common electron chemical potential. (iii) The resulting dipole layer creates a step in the electrostatic potential across the metal/molecule interface (white-and-black contour), which pushes the HOMO back down below  $E_F$ . The reverse argument holds for the lowest unoccupied molecular orbital. (b) Similar considerations lead to the pinning of the singly occupied molecular orbital (SOMO) of a monoradical to the Fermi level (see text for details). Symmetric reasoning holds for the situation where the SOMO initially lies below  $E_F$ .

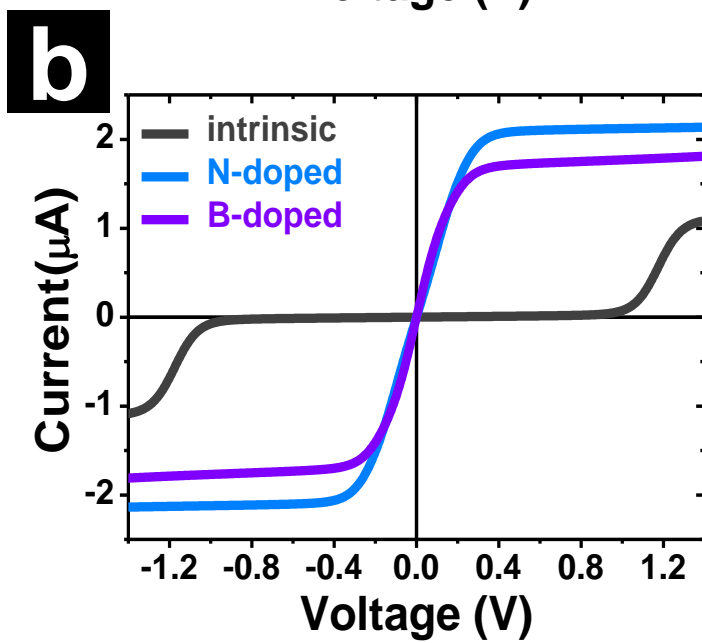
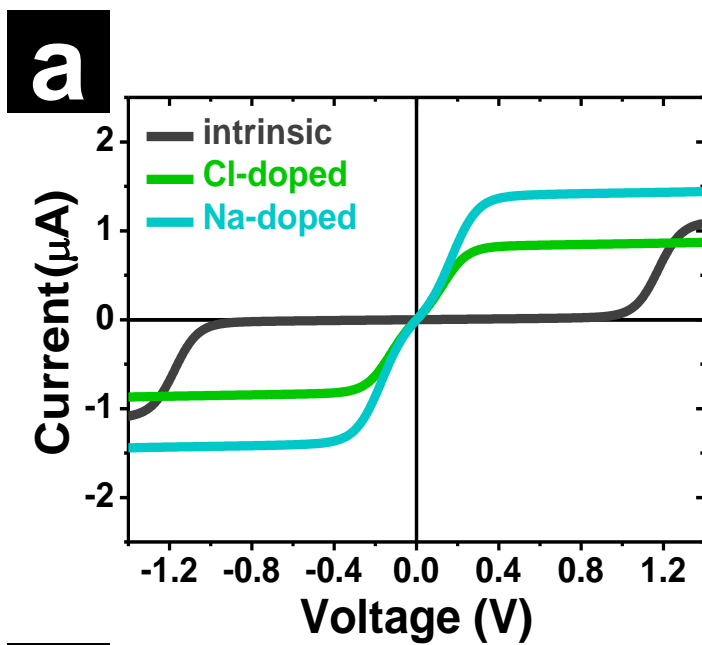
**Figure 5.** (a) Calculated density of states projected onto the molecular region (PDOS) of the junction containing the N-doped (blue) and B-doped (violet) neutral radicals (center); the vertical axis with its origin at the common Fermi level ( $E_F$ ) of the system represents energy in eV. The left panels show the local density of states (LDOS) integrated over an energy window of  $\pm 30$  meV around the HOMO-derived peak in the PDOS (bottom, red) and around  $E_F$  (top, orange) in the case of N-doping. The right panels show the LDOS integrated over an energy window of  $\pm 30$  meV around  $E_F$  (bottom, orange) and the LUMO-derived peak in the PDOS (top, blue) for the B-doped case.

**Figure 1** (*single column*)



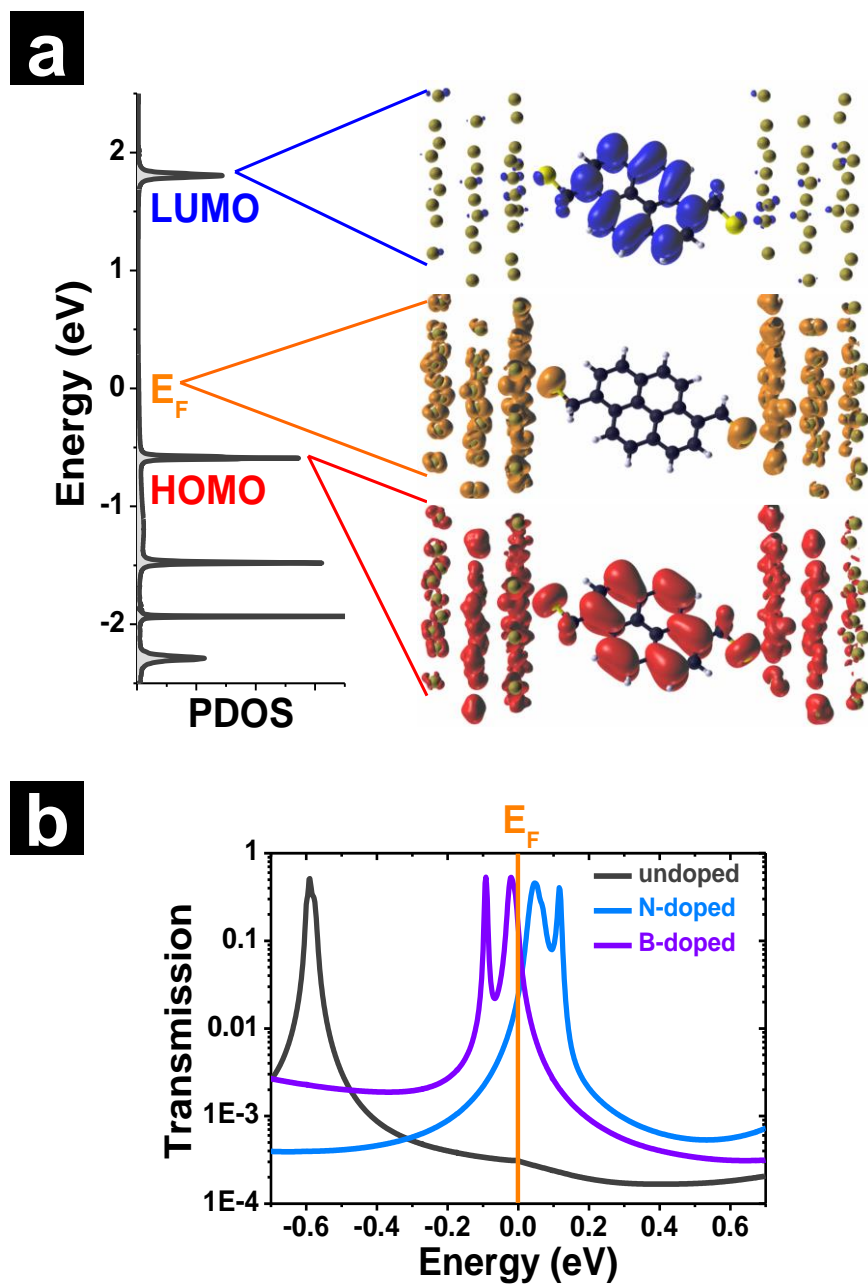
G. Heimel *et al.*

**Figure 2** (*single column*)



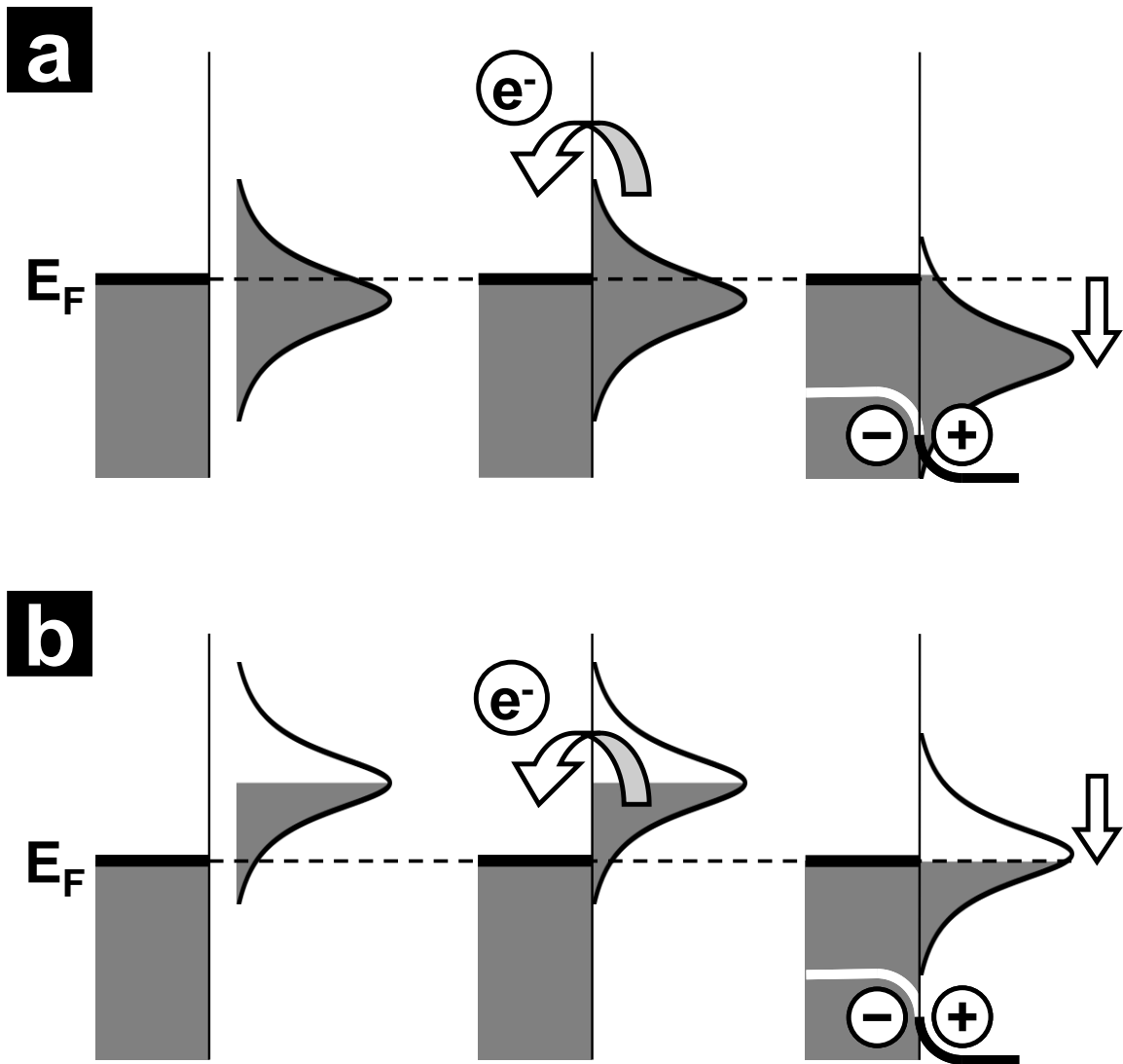
G. Heimel *et al.*

**Figure 3** (*single column*)



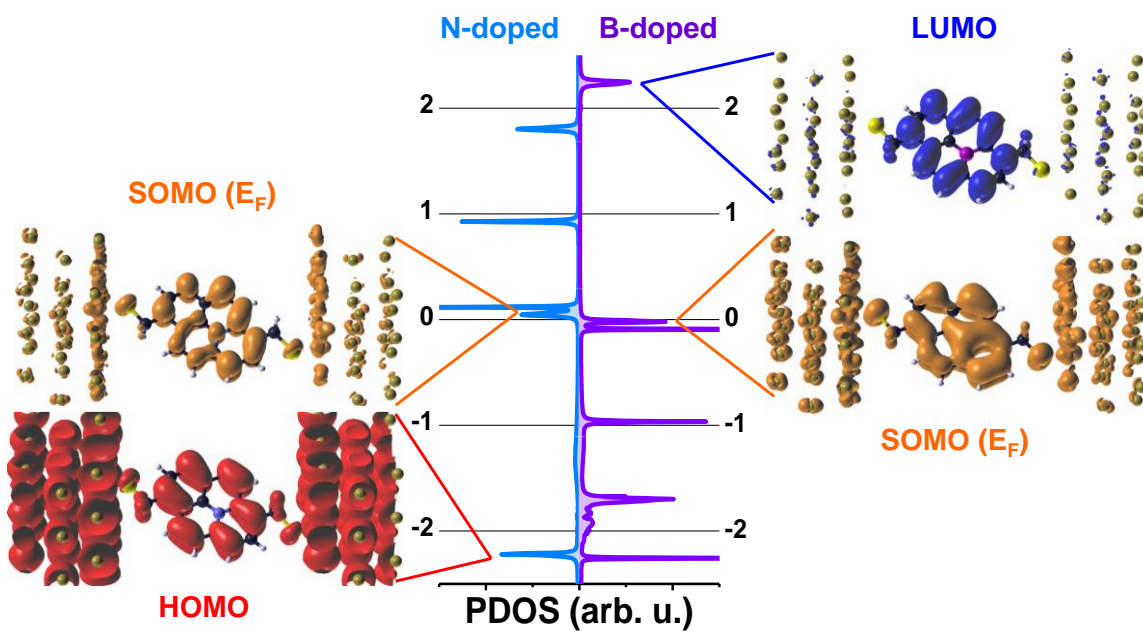
G. Heimel *et al.*

**Figure 4** (*single column*)



G. Heimel *et al.*

**Figure 5** (*double column*)



G. Heimel *et al.*